Electronic Supplementary Material (ESI) for Journal of Materials Chemistry A.


# Vacancy-engineered $CeO_2$/Co heterostructure anchored on the nitrogen-doped porous carbon nanosheet arrays vertically grown on carbon cloth as an integrated cathode for oxygen reaction of rechargeable Zn-air battery

*Shuxin Li,[a,b] Han Zhang,*[a,b] Lin Wu,[a,b] Hongwei Zhao,[a,b] Lixiang Li,*[a,b] Chengguo Sun[a,b] and Baigang An*[a,b]*

[a] School of Chemical Engineering, University of Science and Technology Liaoning, Anshan 114051, China.

[b] Key Laboratory of Energy Materials and Electrochemistry Research Liaoning Province, Anshan 114051, China.

*E-mail addresses: hzhang0807@163.com (H. Zhang), lxli2005@126.com (L. Li), bgan@ustl.edu.cn (B. An).

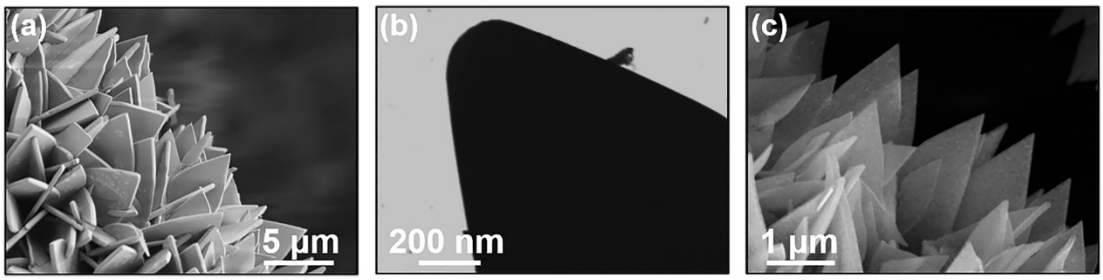


**Fig. S1.** (a) SEM and (b) TEM images of Co-MOF@CC. (c) SEM image of Co-NCNA@CC.

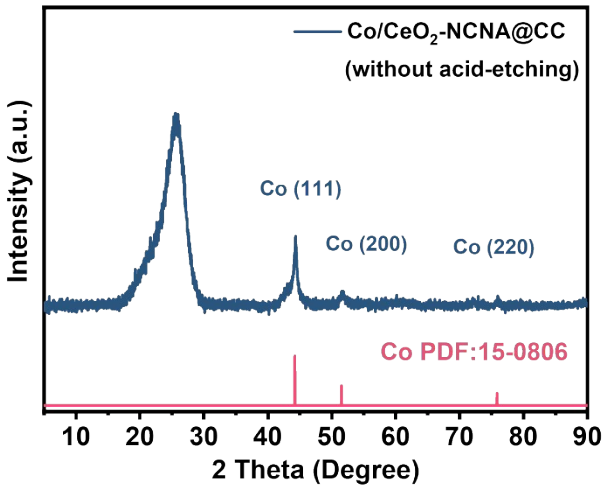


**Fig. S2.** XRD patterns of $Co/CeO_2$-NCNA@CC without the acid-etching.

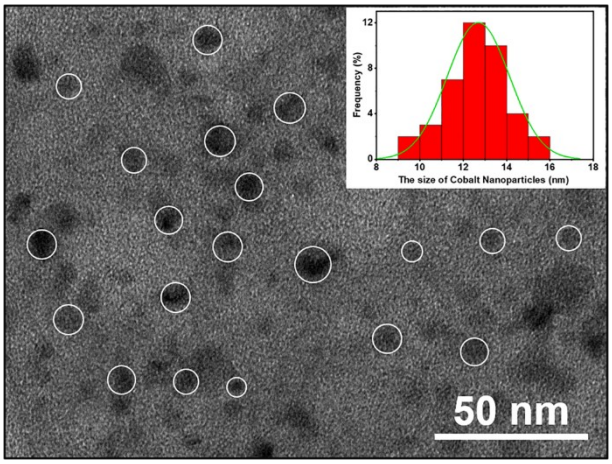


**Fig. S3.** TEM image of Co-NCNA@CC. Inset is normal distribution plot of Co nanoparticles in Co-NCNA@CC.

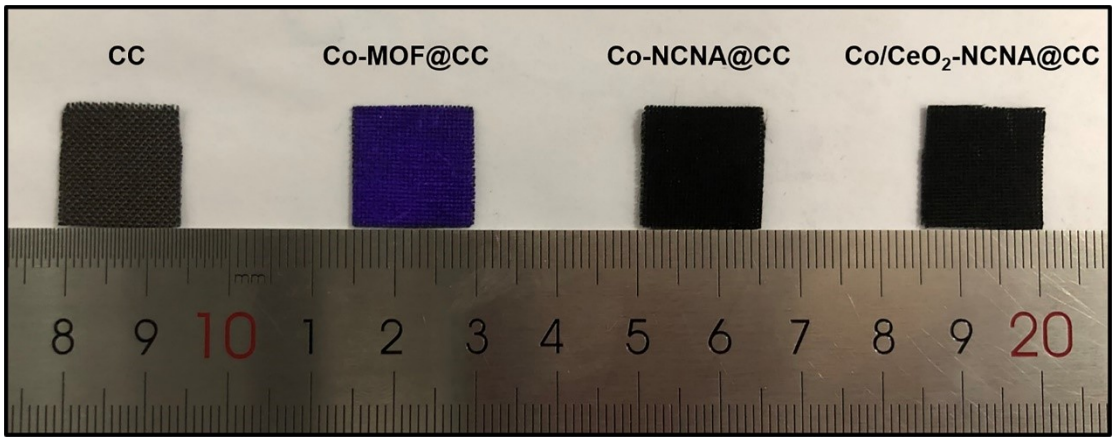


**Fig. S4.** A digital photograph of CC, Co-MOF@CC, Co-NCNA@CC and $Co/CeO_2$-NCNA@CC.

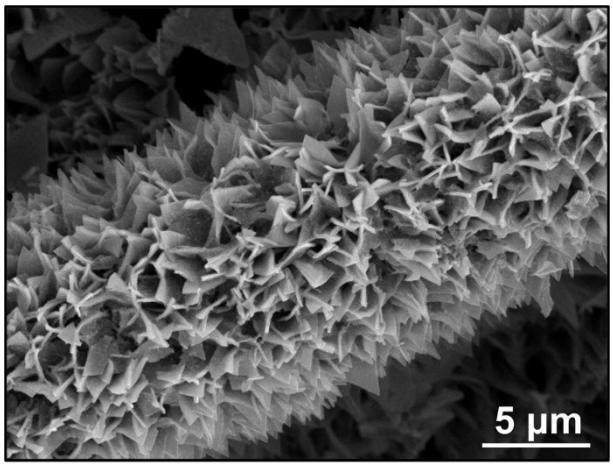


**Fig. S5.** SEM image of Co/$CeO_2$-NCNA@CC.

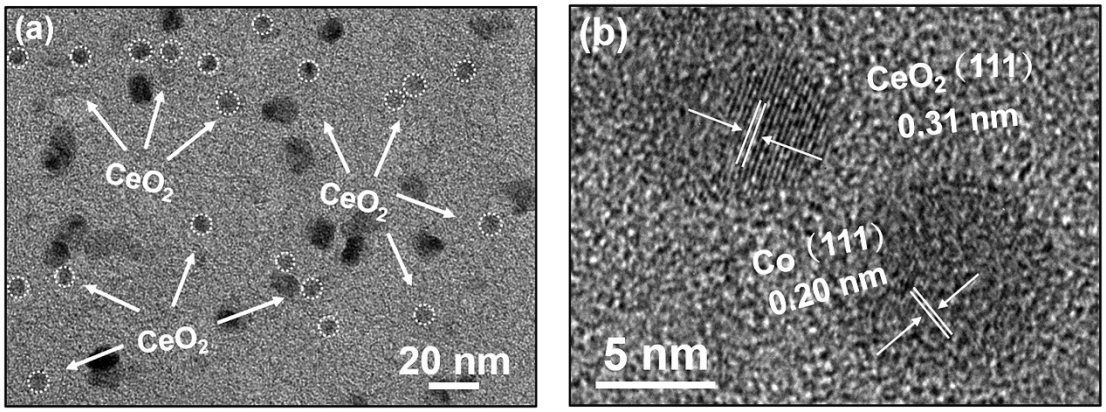


**Fig. S6.** (a) TEM and (b) HRTEM images of Co/$CeO_2$-NCNA@CC.

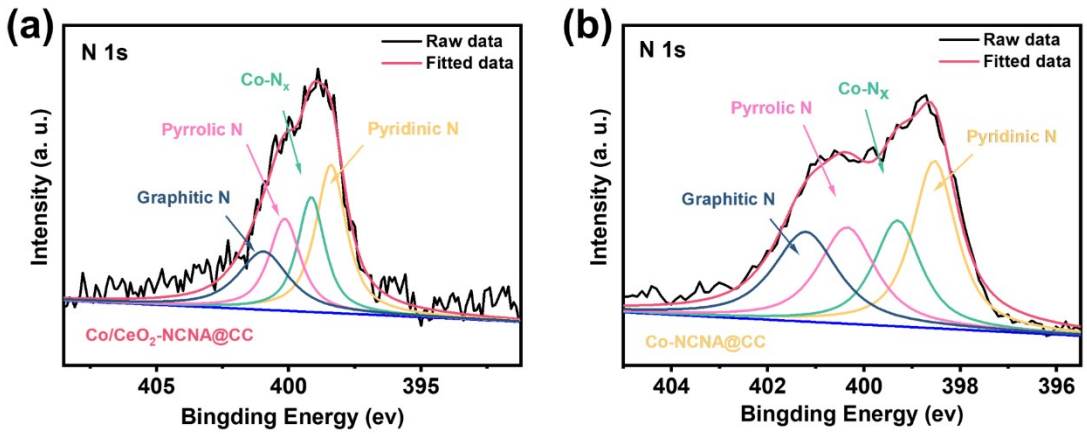


**Fig. S7.** High resolution N 1s XPS spectra of (a) Co/$CeO_2$-NCNA@CC and (b) Co-NCNA@CC.

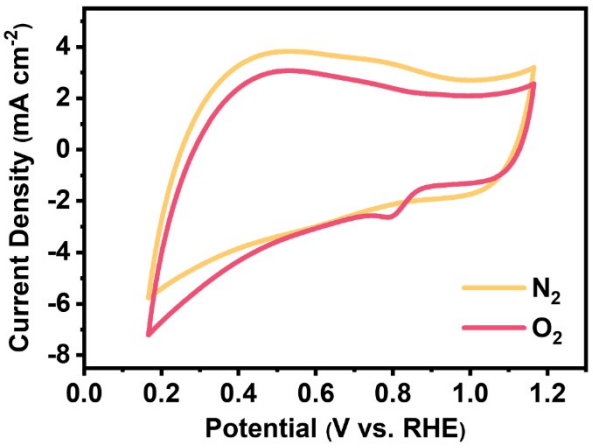


**Fig. S8.** CV curves of $Co/CeO_2$-NCNA@CC in $O_2$ and $N_2$ saturated 0.1 M KOH.

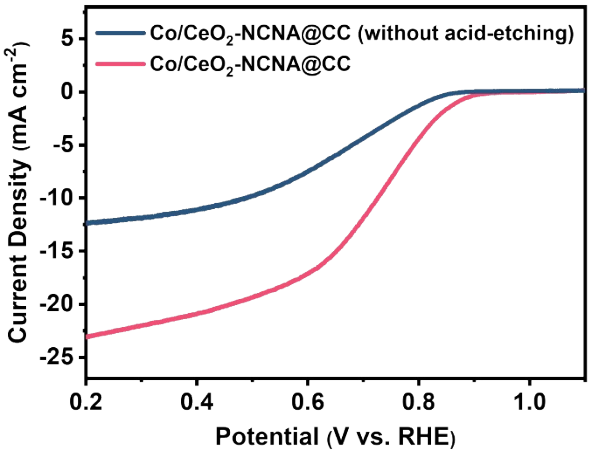


**Fig. S9.** LSV curves of the Co/$CeO_2$-NCNA@CC catalysts with and without the acid-etching.

Compared the ORR polarization curves of the Co/$CeO_2$-NCNA@CC with and without acid-etching, the sufficient improvement on the ORR activity of Co/$CeO_2$-NCNA@CC can be obtained by the acid-etching.

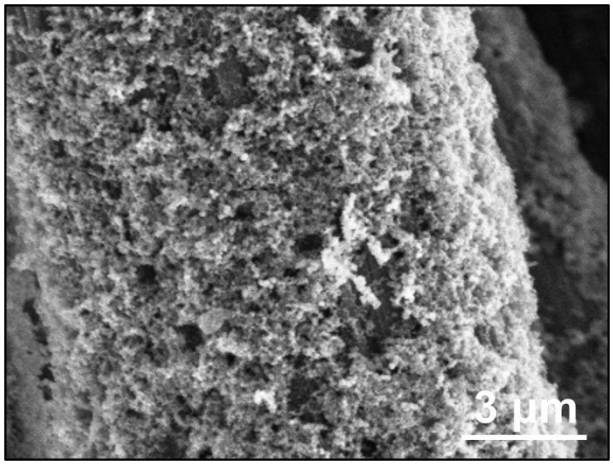


**Fig. S10.** SEM image of Pt/C drop casted onto CC.

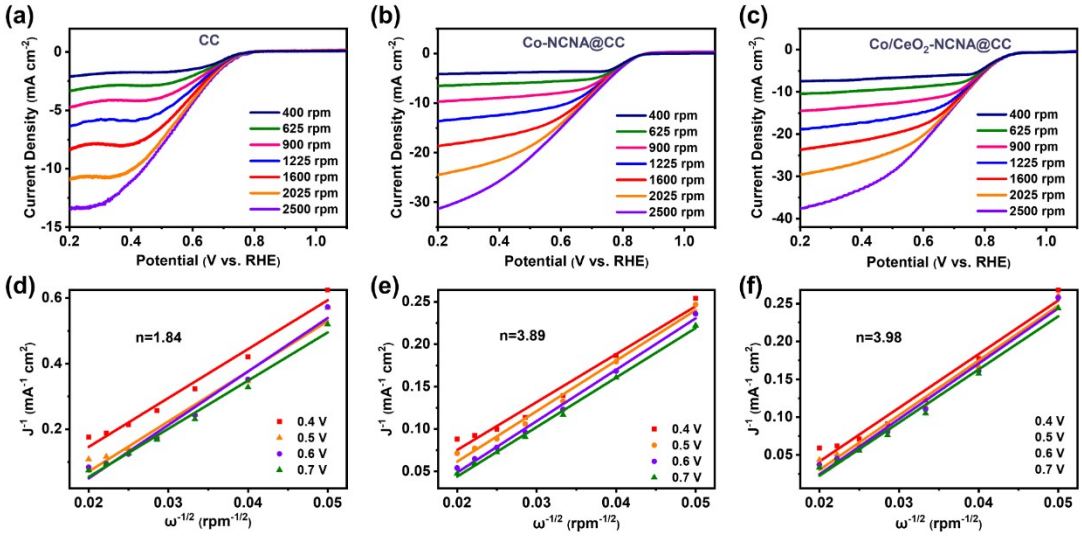


**Fig. S11.** (a, b and c) LSV curves of CC, Co-NCNA@CC and Co/$CeO_2$-NCNA@CC obtained in 0.1 M KOH electrolyte with different scanning rates from 400 to 2500 rpm and (d, e, f) corresponding K-L plots.

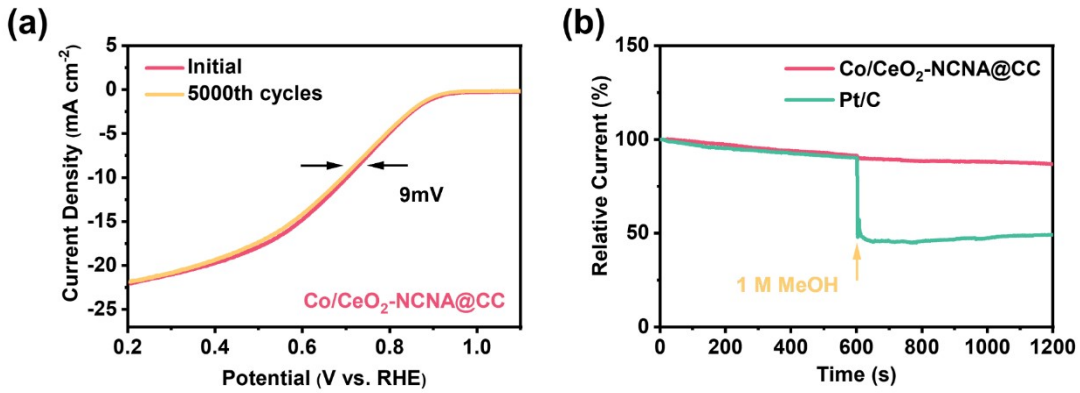


**Fig. S12.** (a) LSV curves of $Co/CeO_2$-NCNA@CC before and after 5000 cycles. (b) Methanol tolerance tests carried out by chronoamperometry with $Co/CeO_2$-NCNA@CC and 20% Pt/C in $O_2$-saturated 0.1 M KOH.

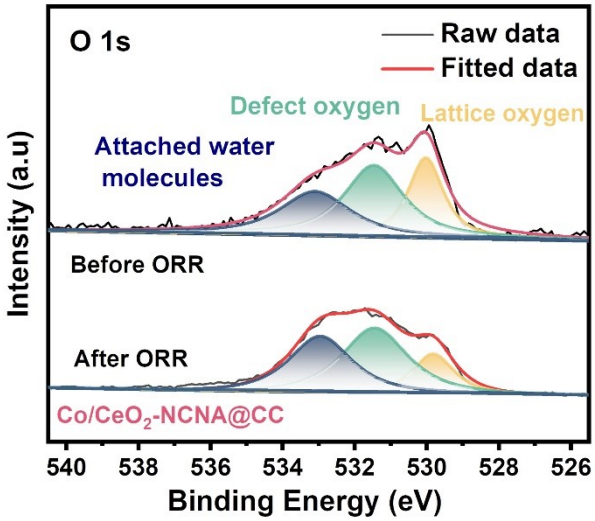


**Fig. S13.** High-resolution XPS spectra of O 1s for $Co/CeO_2$-NCNA@CC before and after the ORR tests.

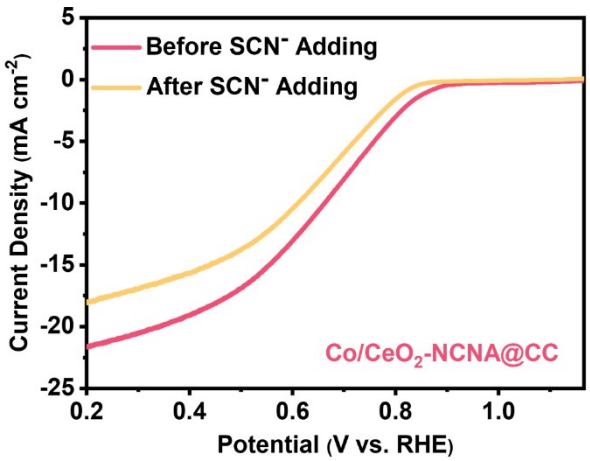


**Fig. S14.** The LSV curves before and after the adding of $SCN^-$.

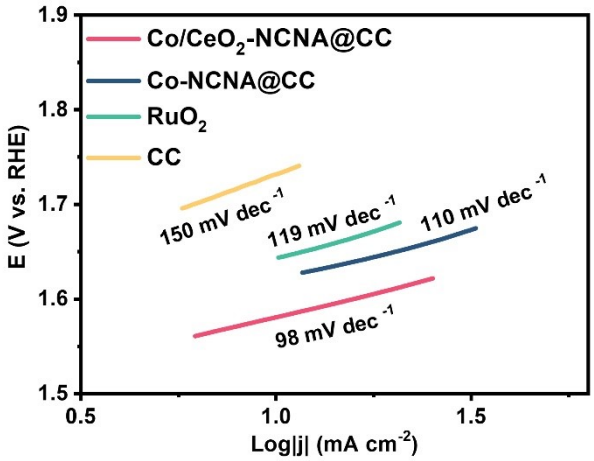


**Fig. S15.** Tafel plots derived from the OER polarization curves of $Co/CeO_2$-NCNA@CC, Co-NCNA@CC, CC and $RuO_2$ catalysts.

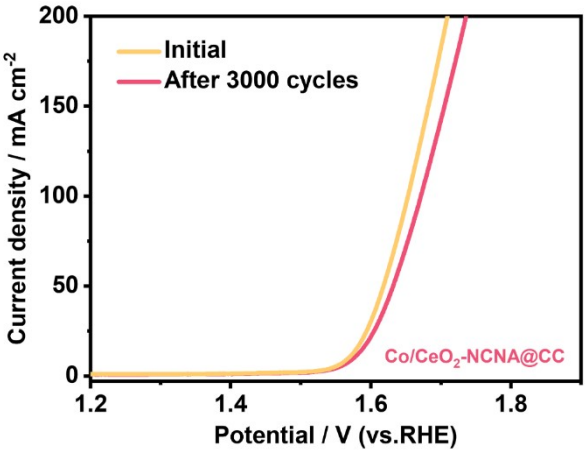


**Fig. S16.** OER polarization plots of $Co/CeO_2$-NCNA@CC catalysts before and after 3000 potential cycles.

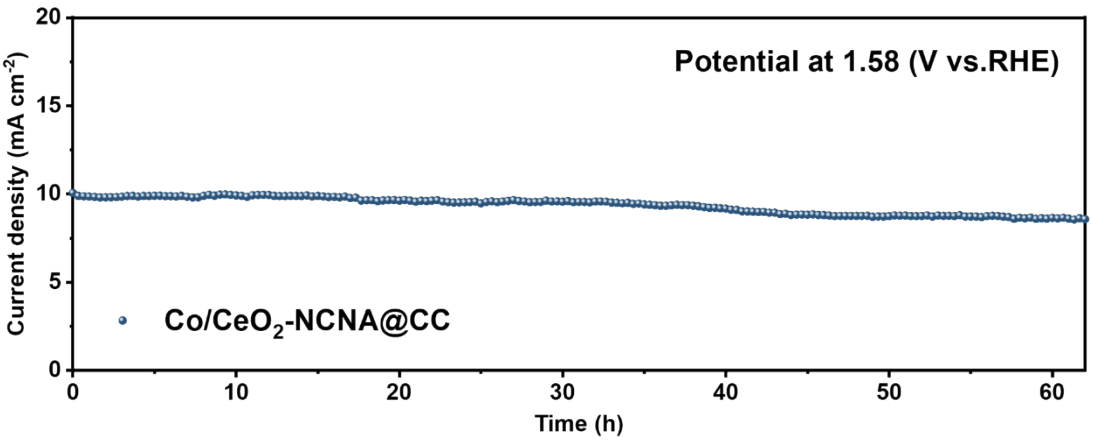


**Fig. S17.** Stability tests of $Co/CeO_2$-NCNA@CC at 1.58 V by chronoamperometry.

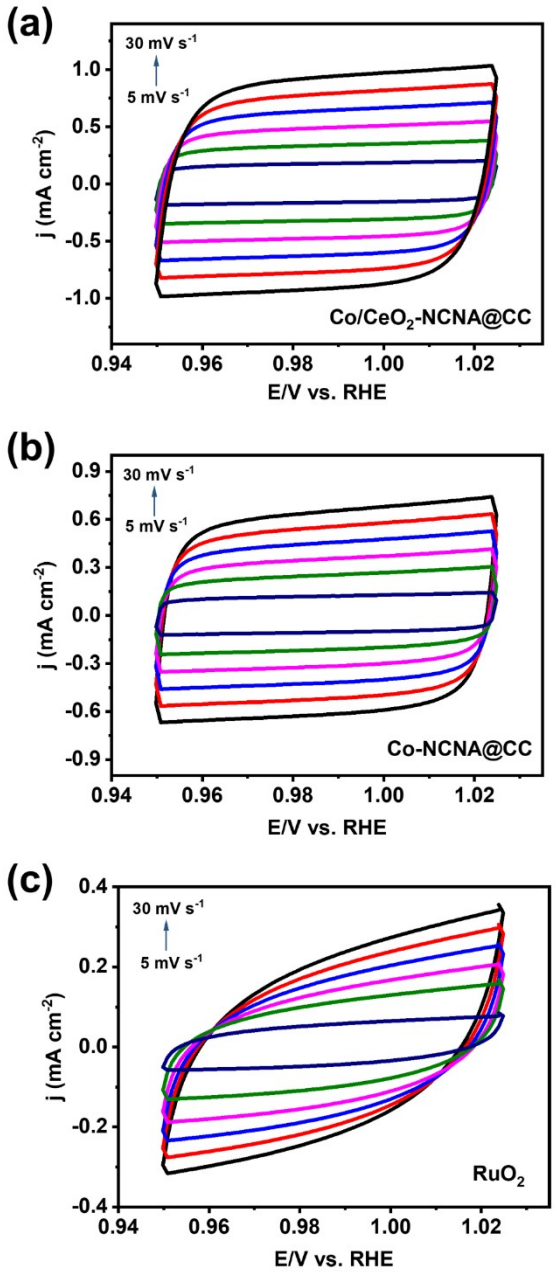


**Fig. S18.** Cyclic voltammograms with various scan rates from 5 to 30 mV $s^{-1}$ of (a) $Co/CeO_2$-NCNA@CC, (b) Co-NCNA@CC, and (c) $RuO_2$.

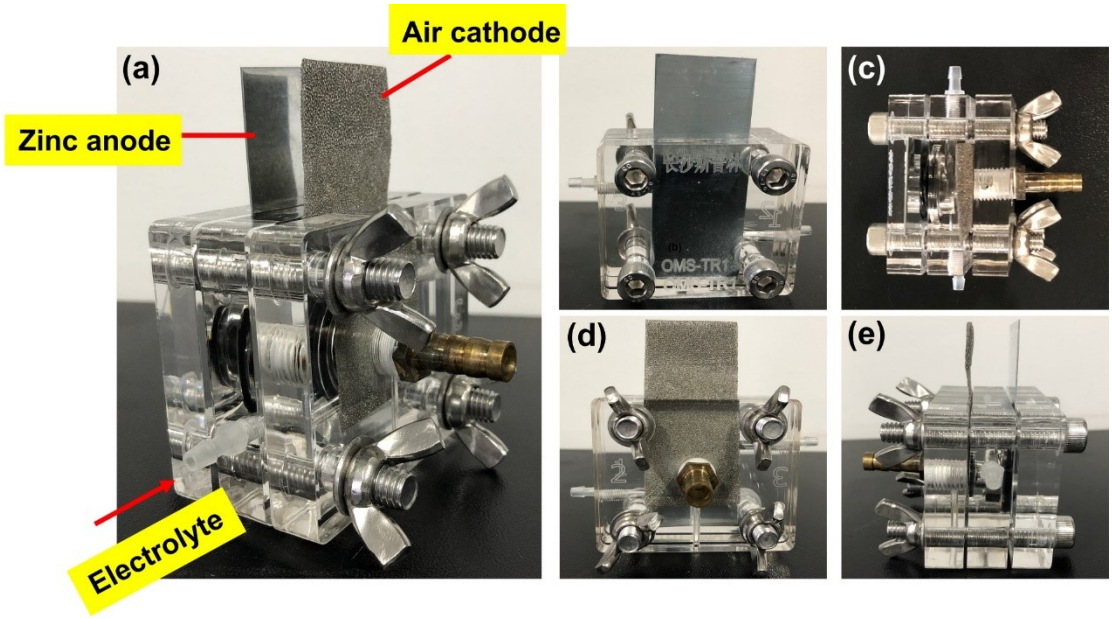


**Fig. S19.** (a-e) Photographs of the rechargeable Zn-air battery recorded from different directions.

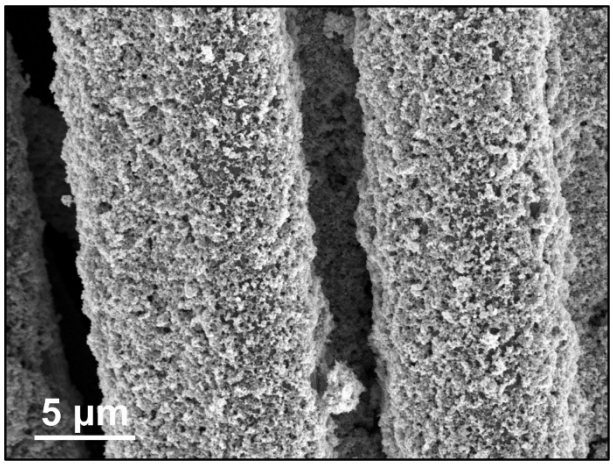


**Fig. S20.** SEM image of Pt/C+$RuO_2$ drop casted onto CC.

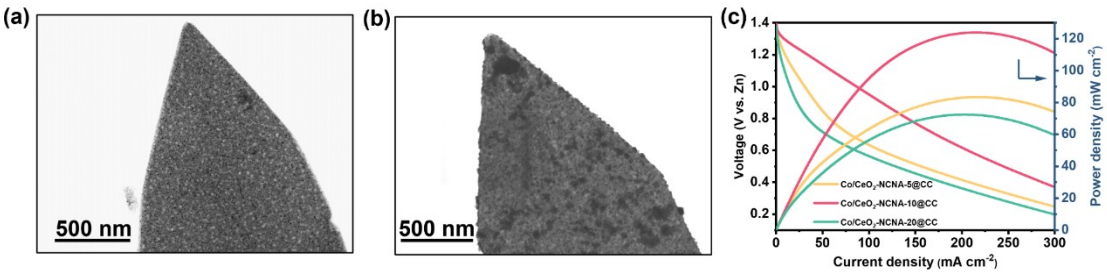


**Fig. S21.** TEM images of (a) Co/$CeO_2$-NCNA-5@CC and (b) Co/$CeO_2$-NCNA-20@CC. (c) Discharging polarization curves and corresponding power density plots of the Zn–air batteries with Co/$CeO_2$-NCNA-5@CC, Co/$CeO_2$-NCNA-10@CC and Co/$CeO_2$-NCNA-20@CC.

When the load of $CeO_2$ reduced to 5 mg, lower density of $CeO_2$ nanocrystals, as well as small nanoparticles, were achieved on Co/$CeO_2$-NCNA-5@CC (Fig. S21a). However, when the load of $CeO_2$ increased to 20 mg, $CeO_2$ nanocrystals with lager nanoparticles and obvious agglomeration appear (Fig. S21b), which will decrease the performance of catalysts (Fig. S21c).

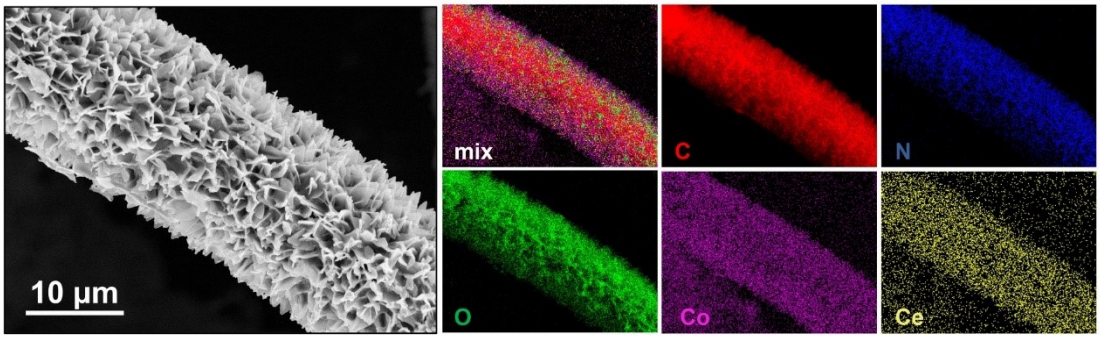


**Fig. S22.** SEM images and element mapping of C, N, O, Co, and Ce of $Co/CeO_2$-NCNA@CC after the Zn–air batteries discharge–charge cycling tests.

The surface composition distribution of the $Co/CeO_2$-NCNA@CC after galvanostatic discharge-charge cycling was measured by EDS elemental mappings. The elemental mapping results reveal cobalt and cerium element evenly distributed on the surface of nanosheet arrays, indicating their excellent stability and phase stability after cycling process.

**Table S1.** Co and Ce contents analysis of Co-NCNA@CC and Co/$CeO_2$-NCNA@CC sample by inductively coupled plasma (ICP) measurement.

| Samples | Co (wt%) | Ce (wt%) |
|---|---|---|
| Co-NCNA@CC | 0.81 | --- |
| Co/$CeO_2$-NCNA@CC | 0.76 | 1.03 |

**Table S2.** The relative contents of elements in $Co/CeO_2$-NCNA@CC and Co-NCNA@CC sample derived from XPS data.

| Elements (wt.%) / Samples | **C** | **N** | **O** | **Co** | **Ce** |
|---|---|---|---|---|---|
| $Co/CeO_2$-NCNA@CC | 81.47 | 3.15 | 9.23 | 2.73 | 3.42 |
| Co-NCNCA@CC | 85.46 | 4.41 | 6.87 | 3.26 | --- |

**Table S3.** EIS data of different samples.

| Sample | $R_s$ | $R_{ct}$ |
|---|---|---|
| Co/$CeO_2$-NCNA@CC | 2.236 | 24.61 |
| Co-NCNA@CC | 2.802 | 45.27 |
| $RuO_2$ | 2.827 | 36.42 |

**Table S4.** Zn-air batteries performance of some previous literature of nonprecious metal catalysts in 6.0 M KOH.

| Air catalysts | Open circuit potential (V) | Power density (mW $cm^{-2}$) | Specific capacity ($mAh \cdot g^{-1}_{Zn}$) | Durability (h) | Ref. |
|---|---|---|---|---|---|
| $Co/CeO_2$-NCNA@CC | 1.47 | 123 | 784 | 380 | This work |
| Co@SNHC | 1.48 | 105 | 708 | 72 | S1 |
| MOF(Co)/C(3:1)-500 | 1.43 | 91 | 620 | 6 | S2 |
| Fe/Co-N/S-C | 1.39 | 103 | - | 27 | S3 |
| Co@NPCFs | 1.44 | 98 | 611 | 80 | S4 |
| NiO/CoN | 1.46 | 80 | 690 | 8 | S5 |
| nNiFe LDH/3D MPC | 1.51 | 97 | 537 | - | S6 |
| $YF_3$@NC | 1.47 | 75 | 620 | - | S7 |
| NPCS-900 | - | 79 | 684 | 56 | S8 |
| $CoCe\text{-}600N_2$ | 1.41 | 117 | 634 | - | S9 |
| $Fe\text{-}Co_4N$@N-C | 1.46 | 105 | 806 | 36 | S10 |
| Co@N-HPC-800 | 1.42 | 89 | - | 25 | S11 |

## References


S1 J. Liu, L. Xu, Y. Deng, X. Zhu, J. Deng, J. Lian, J. Wu, J. Qian, H. Xu, S. Yuan, H. Li, P. M. Ajayan, J. Mater. Chem. A, 2019, 7, 14291-14301.

S2 X. Yi, X. He, F. Yin, B. Chen, G. Li, H. Yin, *Electrochim. Acta*, 2019, **295**, 966-977.

S3 C. Li, H. Liu, Z. Yu, *Appl. Catal. B Environ.*, 2019, **241**, 95-103.

S4 Y. Chen, W. Zhang, Z. Zhu, L. Zhang, J. Yang, H. Chen, B. Zheng, S. Li, W. Zhang, J. Wu, F. Huo, *J. Mater. Chem. A*, 2020, **8**, 7184-7191.

S5 J. Yin, Y. Li, F. Lv, Q. Fan, Y.-Q. Zhao, Q. Zhang, W. Wang, F. Cheng, P. Xi, S. Guo, *ACS Nano*, 2017, **11**, 2275-2283.

S6 W. Wang, Y. Liu, J. Li, J. Luo, L. Fu, S. Chen, *J. Mater. Chem. A*, 2018, **6**, 14299-14306.

S7 W. Wang, Y. Mi, Y. Kang, X. Liu, S. Imhanria, Z. Lei, *J. Power Sources*, 2020, **472**, 228451.

S8 S. Chen, L. Zhao, J. Ma, Y. Wang, L. Dai, J. Zhang, *Nano Energy*, 2019, **60**, 536-544.

S9 X. He, X. Yi, F. Yin, B. Chen, G. Li, H. Yin, *J. Mater. Chem. A*, 2019, **7**, 6753-6765.

S10 Q. Xu, H. Jiang, Y. Li, D. Liang, Y. Hu, C. Li, *Appl. Catal. B Environ.*, 2019, **256**, 117893.

S11 Y. Liu, Z. Chen, N. Zhao, G. Tong, Z. Li, B. Wang, Y. Du, Q. Pan, Z. Li, Y. Xie, Y. *Yang*, *Chem. Eng. J.*, 2022, 433, 134469.